

Article

A Computational Study of the Immobilization of New 5-Nitroisatine Derivatives with the Use of C60-Based Functionalized Nanocarriers

Przemysław Czeleń ^{1,*} , Beata Szefler ¹  and Agnieszka Skotnicka ² 

¹ Department of Physical Chemistry, Faculty of Pharmacy, Collegium Medicum, Nicolaus Copernicus University, Kurpiskiego 5, 85-096 Bydgoszcz, Poland

² Faculty of Chemical Technology and Engineering, Bydgoszcz University of Science and Technology, Seminaryjna 3, 85-326 Bydgoszcz, Poland

* Correspondence: przemekcz@cm.umk.pl

Abstract: Isatin-based compounds are a large group of drugs used as competitive inhibitors of ATP. The 5-nitroisatin derivatives studied in this work are inhibitors of the CDK2 enzyme, which can be used in the development of new anti-cancer therapies. One of the basic activities that often allows for an increase in biological activity while reducing the undesirable effects associated with the toxicity of medicinal substances is immobilization based on carriers. In this work, fifty nanocarriers derived from C60 fullerene, containing a bound phenyl ring on their surfaces, were used in the process of the immobilization of isatin derivatives. Based on flexible docking methods, the binding capacities of the drugs under consideration were determined using a wide range of nanocarriers containing symmetric and asymmetric modifications of the phenyl ring, providing various types of interactions. Based on the data collected for each of the tested drugs, including the binding affinity and the structure and stability of complexes, the best candidates were selected in terms of the type of substituent that modified the nanoparticle and its location. Among the systems with the highest affinity are the dominant complexes created by functionalized fullerenes containing substituents with a symmetrical location, such as R₂-R₆ and R₃-R₅. Based on the collected data, nanocarriers with a high potential for immobilization and use in the development of targeted therapies were selected for each of the tested drugs.

Keywords: CDK2; isatin derivatives; docking; C60 fullerene derivatives; symmetric and asymmetric C60 fullerene functionalization; drug immobilization



Citation: Czeleń, P.; Szefler, B.; Skotnicka, A. A Computational Study of the Immobilization of New 5-Nitroisatine Derivatives with the Use of C60-Based Functionalized Nanocarriers. *Symmetry* **2023**, *15*, 226. <https://doi.org/10.3390/sym15010226>

Academic Editors:

George Papageorgiou and
Miroslav Miletić

Received: 8 December 2022

Revised: 9 January 2023

Accepted: 11 January 2023

Published: 13 January 2023



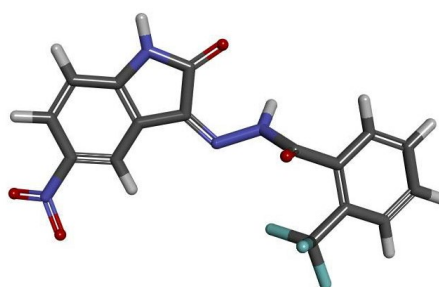
Copyright: © 2023 by the authors. Licensee MDPI, Basel, Switzerland. This article is an open access article distributed under the terms and conditions of the Creative Commons Attribution (CC BY) license (<https://creativecommons.org/licenses/by/4.0/>).

1. Introduction

The isatin molecule provides a convenient platform for the development of a wide range of drugs used to treat a broad variety of diseases [1,2]. Its specific chemical structure ensures high reactivity, and the products of various reactions of this compound have a significant inhibitory capacity against numerous enzymes involved in the regulation of various cellular processes. The inhibitory activity is manifested by the very diverse biological actions of isatin derivatives, including anti-cancer [3–8], anti-bacterial [9], anti-viral [3,10], anti-tuberculous [11,12], anti-malarial [13], and anti-convulsant [14,15] activities. The anti-cancer activity of isatin derivatives is largely related to the ability to inhibit enzymes belonging to the group of cyclin-dependent kinases, which play a key role in regulating the processes of cell division; their overexpression is one of the mechanisms driving the development of cancer [16]. The most important of the enzymes included in this group is cyclin-dependent kinase 2 (CDK2), since many studies clearly confirm its key role in the development of cancer. Numerous studies have clearly established the binding mechanism of drugs containing the isatin core [17–19] to the active site of this protein and have proven their effectiveness in inhibiting the development of neoplastic

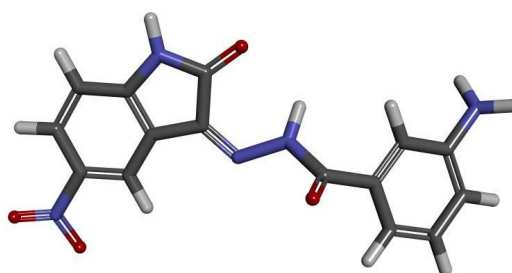
diseases [7,20,21]. The subjects of this study are 5-nitroisatin derivatives, formed in a reaction with substituted benzoylhydrazides. The structures of these compounds are shown in Figure 1. The proposed molecules are competitive inhibitors of the CDK2 enzyme, and their biological activity predisposes them as potential drugs in the development of new anti-cancer therapies [22]. Based on the isatin core, the structural similarity of the proposed compounds to the currently used drugs may contribute to a low selectivity in the context of interactions with the active centers of a wide range of enzymes, which is not always a desirable phenomenon. It seems advisable to propose actions that may affect the biological activity and bioavailability of the considered inhibitors. In such situations, diverse strategies are suggested; one of them is the immobilization of drug molecules based on various carriers.

a



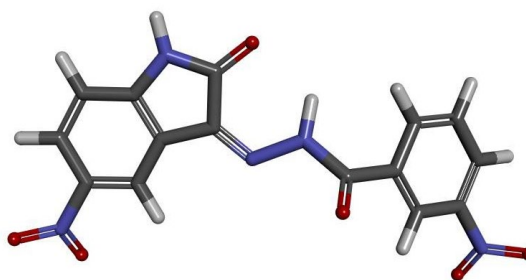
(Z)-N'-(5-nitro-2-oxoindolin-3-ylidene)-2-(trifluoromethyl)benzohydrazide (d1)

b



(Z)-3-amino-N'-(5-nitro-2-oxoindolin-3-ylidene)benzohydrazide (d2)

c



(Z)-3-nitro-N'-(5-nitro-2-oxoindolin-3-ylidene)benzohydrazide (d3)

Figure 1. The graphic representation of 5-NitroIsatin-based drugs used during immobilization process.

This method is often used in the creation of targeted therapies since it allows for the control of the speed and location of drug release. Therefore, it can contribute to extending the release time of active substances [23,24] and, in the case of drugs with a high toxicity, it can reduce undesirable effects [25,26]. A wide spectrum of substances is used in the immobilization process, e.g., albumin [27], polymers [28–30], chitosan [31,32], and hydrogels [33], as well as fullerenes and their derivatives [26,34–36]. Recently, fullerenes have exhibited a very dynamic development and find many applications in medicine and pharmacy. One of the most-exploited molecules in this range is fullerene C60 [26,34–37]. This nanoparticle exhibits good permeation through the cell membrane [38–41] and significant biological

activity. The structure of this nanomolecule supports a high affinity towards all molecules containing aromatic systems. Analogical properties are also shown by the derivatives of C60 molecules, obtained by the addition of diverse chemical groups to increase the binding capabilities of such fullerenes [42,43]. A skillful selection of functional groups used in the functionalization of fullerenes may allow for the acquisition of nanoparticles with a special affinity for specific drugs. A significant increase in the binding capacity of fullerene C60 is obtained after the addition of a single aromatic system [17,44], and the use of further functional groups containing, for example, hydrogen bond donors and acceptors can significantly increase the binding capacity and selectivity of this process. An important group of functionalized fullerenes are nanoparticles modified with chemical groups based on amino acids [42,45]. The structural diversity of such substituents provides a variety of binding agents in the forms of aromatic systems and hydrogen bonds. Such a new class of C60 fullerene derivatives was presented in the previous work [46]. Modifications of the structure of considered fullerenes include a single or multiple substitution of chemical groups to the phenyl ring, leading to the obtainment of all possible symmetrical and asymmetrical configurations of the used substituents. The proposed nanocarriers demonstrated a significant ability to bind drugs containing an isatin core; therefore, it is advisable to determine their suitability for the immobilization of a new group of inhibitors. The development of current methods of computational chemistry allows for a thorough analysis of the properties of compounds with pharmacological potential which is not limited to the description of their basic molecular properties but also allows for the assessment of their impact on potential biological targets, taking into account both their energy and structural aspects [47–50]. The combination of different methods of computational chemistry, taking into account quantum mechanical calculations, docking, or molecular dynamics, can create a comprehensive picture of the studied systems. Their application may allow for the assessment of the possibility of using a selected group of nanocarriers for the immobilization of a new group of the 5-Nitroisatin-based drugs.

2. Materials and Methods

Three 5-nitroisatin derivatives were used in the immobilization process: namely, the d1 (*Z*)-*N'*-(5-nitro-2-oxoindolin-3-ylidene)-2-(trifluoromethyl)benzohydrazide (2b in the source publication), d2 (*Z*)-3-amino-*N'*-(5-nitro-2-oxoindolin-3-ylidene)benzohydrazide (3f in the source publication), and d3 (*Z*)-3-nitro-*N'*-(5-nitro-2-oxoindolin-3-ylidene)benzohydrazide (3h in the source publication) molecules, all of which exhibit a high potential for the inhibition of the CDK2 enzyme [22]. During the immobilization processes, functionalized C60 fullerene derivatives were used. Each nanocarrier molecule considered was created based on the CID_71619159 molecule obtained from the PubChem database [51]. The molecular core of the nanomolecules consisted of a C60 molecule with a single phenyl ring bound to its surface. The modifications introduced in the analyzed systems were associated with the addition of chemical groups to the phenyl ring. The chemical structures of all used nanomolecules are presented in Figure 2. The detailed procedure for creating these nanocarriers was described in the previous work [46]. The immobilization of the considered drugs was realized with the use of singly, doubly, and triply substituted C60 fullerene derivatives. Including all chemical groups presented in Figure 2, a total of 49 different functionalized fullerenes (FFs) were used in the immobilization process. As a reference system, the C60 fullerene was used with a single, nonmodified phenyl ring bound to its surface (C60_phen).

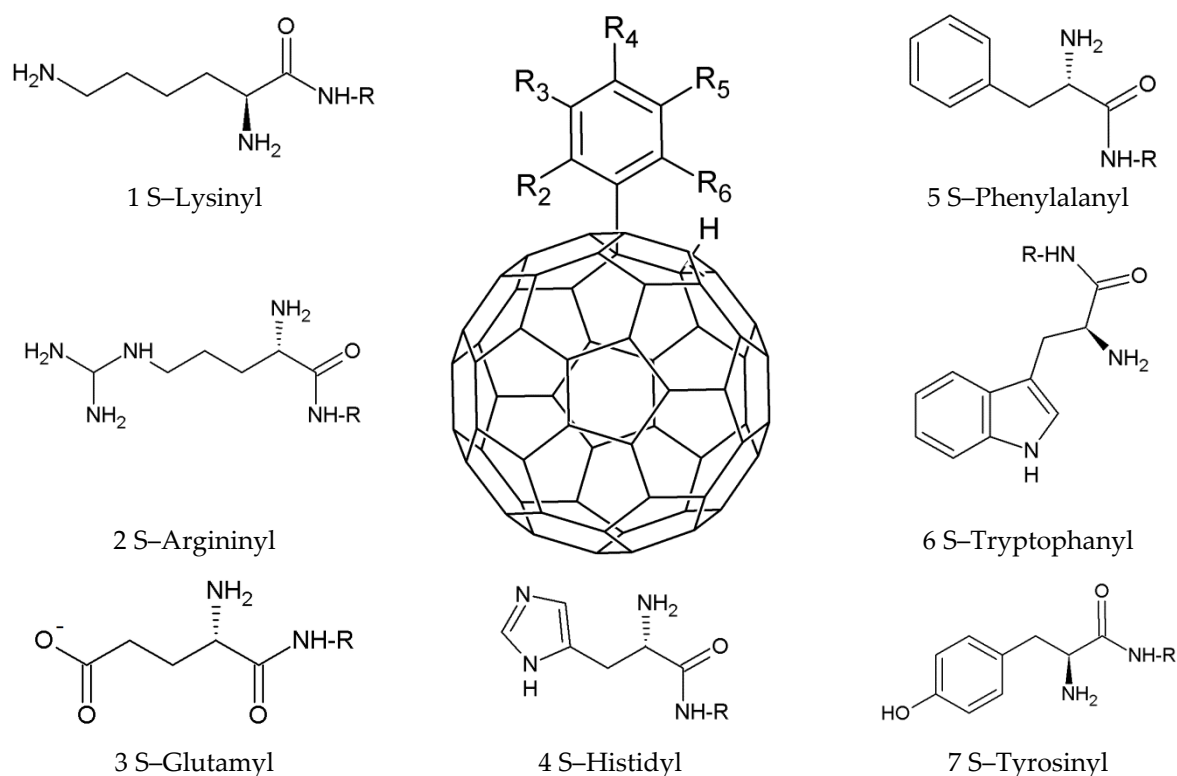


Figure 2. The graphic representation of functionalized C₆₀ fullerene derivatives (FFs). The Rx descriptions define the place of addition of the substituent. The numbers from 1 to 7 define particular substituents.

2.1. DFT Computational Details

The geometric optimization of the drugs considered was realized based on the density functional theory with the use of B3LYP [52–54] functional and a 6-311++G(d,p) basis set [55,56]. The calculations were realized with the use of an SCRf (self-consistent reaction field) approach [57] based on the Poisson–Boltzmann equation [58]. All calculations were carried out using Gaussian 09 software [59]. The analysis of electrostatic potential distribution was realized with the use of Multiwfn software [60].

2.2. Docking Procedure

The docking procedure was realized with the use of the AutoDock VINA program, utilizing a united-atom scoring function [61]. In all docking calculations, the chemical structures of functionalized fullerenes and drugs containing only polar hydrogen atoms were used; the rest of the hydrogens were removed. Taking into account the potentially significant rotational capacity of the chemical groups used in the formation of nanoparticles, flexible docking was used. This approach made it possible to obtain the best match of the tested carriers to the drugs under consideration. Each system used during the docking procedure was created by placing a nanomolecule in the center of a cubic grid box with dimensions of 32 × 32 × 32 Å. All the preliminary steps, such as descriptions of the drugs' and nanomolecules' structures and the definition of the grid box dimensions, were realized with the use of the AutoDock Tolls application [62]. During the calculations, in order to ensure adequate reproducibility of the simulation and an acceptable computation time, the value of the exhaustiveness parameter was set to 20. For each of the considered systems, in order to verify the reproducibility of the final structure of the complex, five independent simulations were performed with different random-seed values. The VMD application was used during the structural analysis and the visualization of the representative complexes obtained during the docking stage [63].

3. Results and Discussion

Each of the inhibitors of the CDK2 enzyme considered during the docking stage is a 5-nitroisatin derivative obtained through a reaction with the substituted benzoylhydrazide. In the structure of these compounds, two cyclic systems can be distinguished that are bound by a hydrazinic bond. Each of them contains an aromatic system that may be involved in the formation of stacking interactions with the nanocarrier molecule.

Hydrogen bonds are another important factor that may affect the stabilization of the complexes of the considered drugs with the proposed nanocarriers. The optimized structures of drugs presented in Figure 3 and the distribution of ESP values clearly indicate a large number of potential donors and acceptors of hydrogen bonds. Each of the presented drug molecules is dominated by hydrogen bond acceptors. Taking into account the distribution of the minima for the ESP value, it can be seen that the oxygen atom from the benzoylhydrazine group should have the best hydrogen-bond-acceptor capacity. The binding abilities of the isatin core of the considered drugs seem very similar; this is confirmed by the almost identical ESP values for the nitro groups and the polar hydrogen atom. The only qualitative discrepancies are noticeable for the oxindole oxygen atom. Significantly greater disproportions in terms of potential binding capacity may be caused by functional groups located in the second aromatic system of the tested drugs. The trifluoromethyl group in the d1 derivative is characterized by the presence of a negative potential; however, its ability to form durable hydrogen bonds is insignificant. Another of the considered drugs (d2) has an amino group in position 3 of the second aromatic system that will promote interactions with nanocarriers containing active groups with potential hydrogen-bond acceptors. The last of the tested compounds (d3) has a nitro group that can form hydrogen bonds with hydrogen-bond donors, which are present in many of the substituents that modify the nanoparticles used. Such a high quantity and significant diversity of binding factors should ensure the possibility of creating stable complexes with appropriately fitted nanocarriers. In the presented research, 50 nanocarrier particles were used, including a reference molecule and 49 FFs, which could be divided into seven classes, taking into account both the number of modifications and the type of chemical group used. When considering the data collected for all the analyzed drug molecules a significant regularity was noticed, indicating unequivocally that nanocarriers having a single modification in the phenyl ring show the weakest binding capacity. Unquestionably, the modification in the R_4 position has the least favorable effect on the binding capacity of all considered nanoparticles. A slight increase in these properties is observed for mono-derivatives with substituents located in the R_3 and R_2 positions. The general trends observed for monosubstituted nanocarriers are largely independent of the type of substituent used, but this situation changes if we take into account the classes of nanoparticles with multiple modifications in the phenyl ring. Among all the considered functionalized fullerenes with a greater number of substituents, there are derivatives with substitutions in the R_2 - R_4 positions, for which the observed affinity values for the tested inhibitors are at a level similar to the results obtained for mono-derivatives. In the case of the remaining classes of multi-substituted nanocarriers, an unequivocal gradation cannot be distinguished and the factor determining the binding capacity is not only the location of the substituents but is also mainly the type of the chemical group used, which defines the quantity and type of impacts and enables the occurrence of stabilizing interactions.

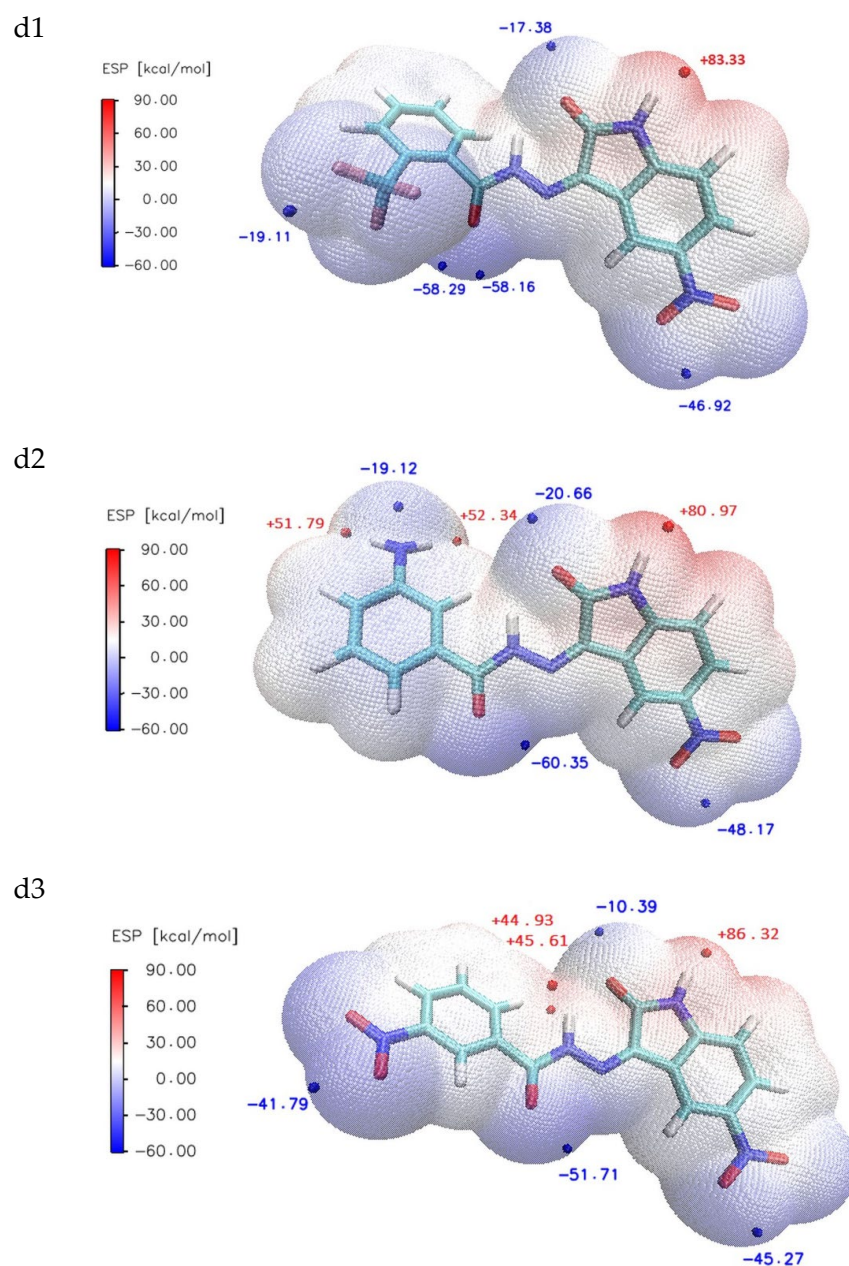


Figure 3. Distributions of ESP values for 5-nitroisatin derivatives estimated in water at the B3LYP/6-311++G(d,p) level of theory. The blue and red points represent the localization of the chosen ESP minima and maxima, respectively.

The values presented in Table 1 show that the d1 molecule creates the most stable complex, with FF containing tryptophanyl substituents in positions R₃-R₅. The modifications of this particular nanocarrier caused a 35-fold increase in binding affinity relative to the reference system. The structure of this complex is presented in Figure 4a. The stability of this system is mainly maintained by stacking interactions, which can be observed between the aromatic systems of the drug molecule, the tryptophanyl substituent, and the surface of C60 fullerene. The isatine core of the drug is involved in the creation of a stacking cluster, located centrally between the fullerene surface and the tryptophan cyclic part. The observed values of the distances between interacting aromatic systems are placed in the range from 3.34 to 3.61 Å (Table 2), indicating the significant strength of such interactions and the important structural consolidation of the considered complex.

Table 1. The values of binding affinity ΔG [kcal/mol] of the d1 molecule toward proposed FFs; K [106] represents values of the binding constant; K_X/K_{C60p} represents normalized factors describing the increase of binding constant relative to the reference structure (C60_phen; $\Delta G = -6.5$ [kcal/mol]; $K = 0.058 \times 10^6$); and K_X/K_{Xmin} represents normalized factors describing the increase of the binding constant relative to the smallest values obtained for functionalized fullerene with a particular substituent.

Localization of Substituents		FF						
		R ₂ -R ₄ -R ₆	R ₂ -R ₄	R ₂ -R ₆	R ₃ -R ₅	R ₂	R ₃	R ₄
S-Lysinyl	ΔG [kcal/mol]	-7.7	-7.4	-7.6	-7.7	-7.3	-6.9	-6.7
	K [$\times 10^6$]	0.44	0.27	0.37	0.44	0.22	0.11	0.08
	K_X/K_{C60p}	7.58	4.57	6.40	7.58	3.86	1.96	1.40
	K_X/K_{Xmin}	5.41	3.26	4.57	5.41	2.75	1.40	1.00
S-Argininyll	ΔG [kcal/mol]	-8.5	-7.4	-8.3	-8.1	-7.9	-7.2	-6.8
	K [$\times 10^6$]	1.70	0.27	1.21	0.87	0.62	0.19	0.10
	K_X/K_{C60p}	29.24	4.57	20.86	14.89	10.62	3.26	1.66
	K_X/K_{Xmin}	17.62	2.75	12.58	8.97	6.40	1.96	1.00
S-Glutamyl	ΔG	-7.4	-7.4	-7.3	-7.5	-7.2	-6.9	-6.7
	K [$\times 10^6$]	0.27	0.27	0.22	0.31	0.19	0.11	0.08
	K_X/K_{C60p}	4.57	4.57	3.86	5.41	3.26	1.96	1.40
	K_X/K_{Xmin}	3.26	3.26	2.75	3.86	2.33	1.40	1.00
S-Histidyl	ΔG [kcal/mol]	-7.6	-7.7	-7.5	-7.6	-7	-7.6	-6.7
	K [$\times 10^6$]	0.37	0.44	0.31	0.37	0.14	0.37	0.08
	K_X/K_{C60p}	6.40	7.58	5.41	6.40	2.33	6.40	1.40
	K_X/K_{Xmin}	4.57	5.41	3.86	4.57	1.66	4.57	1.00
S-Phenylalanyl	ΔG [kcal/mol]	-8.4	-7.6	-7.7	-7.8	-7.5	-7	-6.7
	K [$\times 10^6$]	1.44	0.37	0.44	0.52	0.31	0.14	0.08
	K_X/K_{C60p}	24.70	6.40	7.58	8.97	5.41	2.33	1.40
	K_X/K_{Xmin}	17.62	4.57	5.41	6.40	3.86	1.66	1.00
S-Tryptophanyl	ΔG [kcal/mol]	-7.8	-7.3	-8.1	-8.6	-7.8	-7.7	-6.7
	K [$\times 10^6$]	0.52	0.22	0.87	2.01	0.52	0.44	0.08
	K_X/K_{C60p}	20.86	3.86	14.89	34.62	8.97	7.58	1.40
	K_X/K_{Xmin}	6.4	2.75	10.62	24.70	6.40	5.41	1.00
S-Tyrosinyl	ΔG [kcal/mol]	-7.7	-7.4	-7.7	-8.3	-7.7	-7.3	-6.7
	K [$\times 10^6$]	0.44	0.27	0.44	1.21	0.44	0.22	0.08
	K_X/K_{C60p}	7.58	4.57	7.58	20.86	7.58	3.86	1.40
	K_X/K_{Xmin}	5.41	3.26	5.41	14.89	5.41	2.75	1.00

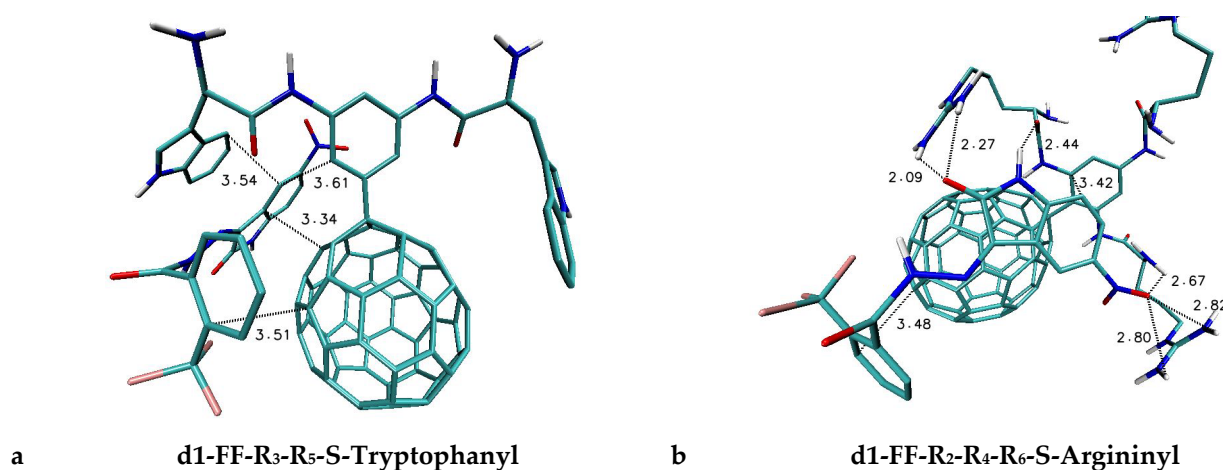


Figure 4. Cont.

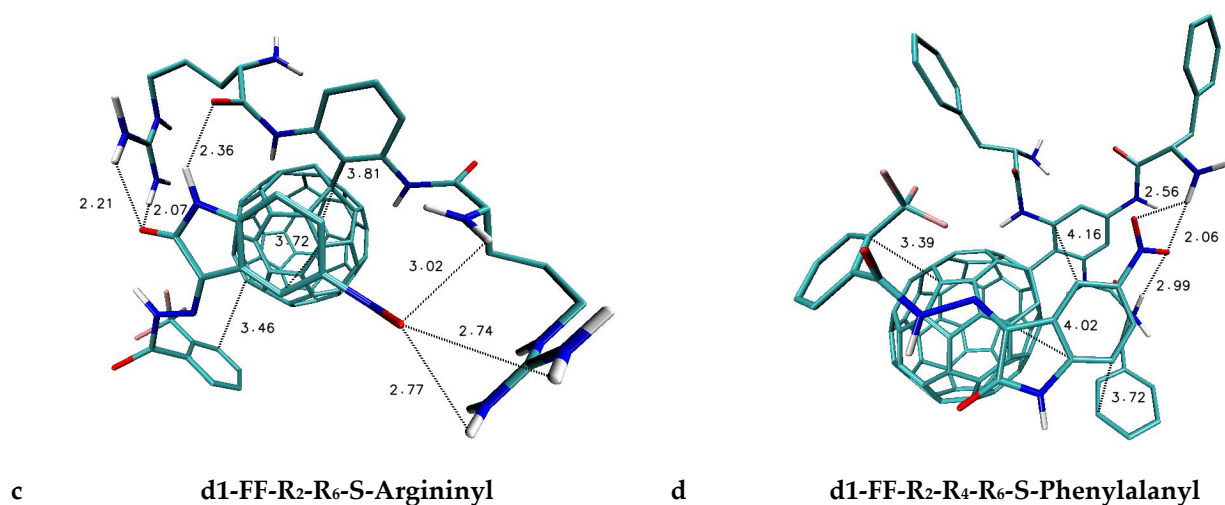


Figure 4. The graphic representation of the chosen complexes created by the d1 molecule with FF characterized by higher values of binding affinity. The atoms of particular chemical elements are indicated by following colors: carbon—cyan; oxygen—red; nitrogen—blue; fluorine—pink; and hydrogen—white.

Table 2. The values of distances [Å] measured between interacting aromatic systems identified in the most stable complexes created by considered drugs with chosen FFs. The interacting subunits are described by the following abbreviations: isat-core—isatin, part of considered drugs; phenyl-ring—aromatic system of the drug molecule belonging to the benzoylhydrazide part of the drug; C60 full-surface—the surface of C60 fullerene; Tryptophanyl and Phenylalanyl—aromatic systems of substituents used in the FFs; and phenyl-ring—aromatic system bound to the fullerene surface.

Drug mol.	Interacting Molecular Subunits Drug—Nanocarrier	Distance [Å]			
		FF-R ₃ -R ₅ -S-Tryptophanyl	FF-R ₂ -R ₄ -R ₆ -S-Argininy	FF-R ₂ -R ₆ -S-Argininy	FF-R ₂ -R ₄ -R ₆ -S-Phenylalanyl
d1	Isat-core—C60full-surf	3.34	3.44	3.72	4.02
	Isat-core—Tryptophanyl	3.54	—	—	—
	Isat-core—phenyl-ring	3.61	3.42	3.81	4.16
	phenyl-ring—C60full-surf	3.51	3.48	3.46	3.39
	Isat-core—Phenylalanyl	—	—	—	3.72
d2		FF-R ₃ -R ₅ -S-Tryptophanyl	FF-R ₂ -R ₄ -R ₆ -S-Argininy	FF-R ₂ -R ₆ -S-Argininy	
	Isat-core—C60full-surf	3.56	3.53	3.52	
	Isat-core—Tryptophanyl	3.58	—	—	
	Isat-core—phenyl-ring	3.89	3.54	3.69	
	phenyl-ring—C60full-surf	3.53	3.53	3.54	
d3		FF-R ₃ -R ₅ -S-Tryptophanyl	FF-R ₂ -R ₄ -R ₆ -S-Argininy	FF-R ₂ -R ₆ -S-Argininy	FF-R ₃ -R ₅ -S-Tyrosiny
	Isat-core—C60full-surf	3.37	3.58	3.55	3.49
	Isat-core—Tryptophanyl	3.62	—	—	—
	Isat-core—phenyl-ring	—	3.73	3.55	3.55
	Pheny-ring—C60full-surf	3.37	3.51	3.71	3.62

The d1 molecule creates two important complexes with FFs containing argininy modifications in positions R₂-R₄-R₆ and R₂-R₆. These two systems exhibit a 29- and 21-fold increase in drug-binding capacity relative to the reference system, respectively. The structures of such complexes are presented in Figure 4a,b, and, in both cases, a conformational orientation of the aromatic systems of the drugs supporting the occurrence of stacking interactions is observed.

Another factor determining the structure and stability of the complexes discussed is the network of hydrogen bonds involving argininy groups that is located in the R₂-R₆ positions and the isatin part of the drug molecule. In the case of both complexes, the presence of at least six hydrogen bonds was found. The distribution of hydrogen bond donors and acceptors in the groups modifying the considered FFs enables a chelating-like binding of the isatine core of the drug molecule.

A significant increase (≈ 25 -fold) in the binding capacity towards the d1 molecule was also noted for an FF with a phenylalanine substituent located in the R₂-R₄-R₆ positions. In the case of this complex (Figure 4d), significant stacking interactions are observed between the aromatic systems of the drug, the fullerene surface, and the phenyl rings of chemical groups localized on the fullerene surface. An additional contribution to the stabilization of the system comes from the hydrogen bonds in which the nitro group is involved. The next analyzed drug—namely, the d2 molecule—creates the most stable complexes with FFs containing arginine modifications in positions R₂-R₄-R₆ and R₂-R₆, for which there is observed a ~ 48 - and ~ 35 -fold increase of binding affinity, respectively, when compared to the reference system (Table 3). The considered complexes are presented in Figure 5a,b. The stability of both systems is maintained by very similar sets of interactions, including stacking interactions observed between all aromatic systems present in the drug and nanocarrier molecules, and also the hydrogen bonds created by substituents localized in R₂-R₆ positions with all the hydrogen-bond acceptors and donors from the isatine core. In the case of these complexes, the oxygen from the benzohydrazide part of the drug molecule is also involved in the creation of such interactions. The hydrogen bonds in both complexes, based on geometric characteristics, can be classified as medium- and weak-strength hydrogen bonds. In the case of the complex created with an FF containing R₂-R₆ modifications, the distances between the hydrogen donors and acceptors are smaller than those reported in the second considered system and are placed in the scope from 1.98 to 2.43 Å. The lower overall affinity value, despite the better quality of hydrogen bonds, may indicate a dominant influence of stacking interactions on the overall affinity value of the considered complexes.

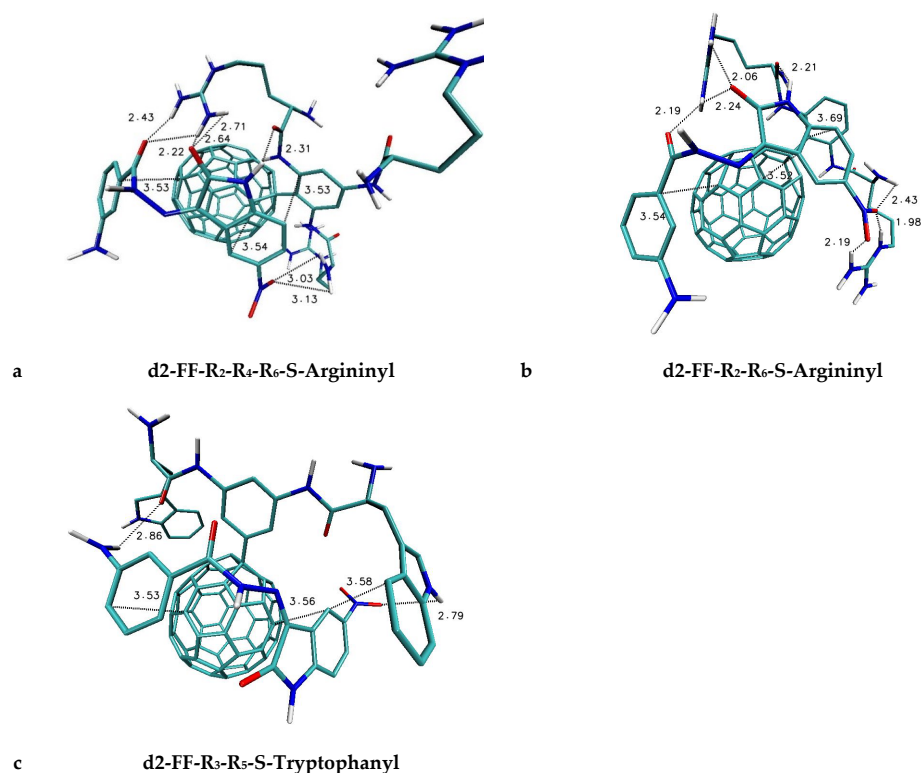


Figure 5. The graphic representation of the chosen complexes created by the d2 molecule with FFs characterized by higher values of binding affinity. The atoms of particular chemical elements are indicated by following colors: carbon—cyan; oxygen—red; nitrogen—blue; and hydrogen—white.

Table 3. The values of the binding affinity ΔG [kcal/mol] of the d2 molecule toward the proposed FFs; K [106] represents values of the binding constant; K_X/K_{C60p} represents normalized factors describing the increase of the binding constant relative to the reference structure (C60_phen; $\Delta G = -6.1$ [kcal/mol]; $K = 0.0296 \times 10^6$); and K_X/K_{Xmin} represents the normalized factors describing the increase of the binding constant relative to the smallest values obtained for functionalized fullerene with a particular substituent.

Localization of Substituents		FF						
		R ₂ -R ₄ -R ₆	R ₂ -R ₄	R ₂ -R ₆	R ₃ -R ₅	R ₂	R ₃	R ₄
S-Lysinyl	ΔG [kcal/mol]	-7.60	-7.30	-7.60	-7.10	-7.00	-6.60	-6.40
	K [$\times 10^6$]	0.37	0.22	0.37	0.16	0.14	0.07	0.05
	K_X/K_{C60p}	12.58	7.58	12.58	5.41	4.57	2.33	1.66
	K_X/K_{Xmin}	7.58	4.57	7.58	3.26	2.75	1.40	1.00
S-Argininyl	ΔG [kcal/mol]	-8.40	-7.30	-8.20	-7.90	-7.20	-7.10	-6.40
	K [$\times 10^6$]	1.44	0.22	1.02	0.62	0.19	0.16	0.05
	K_X/K_{C60p}	48.52	7.58	34.62	20.86	6.40	5.41	1.66
	K_X/K_{Xmin}	29.24	4.57	20.86	12.58	3.86	3.26	1.00
S-Glutamyl	ΔG	-7.30	-7.00	-7.30	-7.30	-6.90	-6.90	-6.20
	K [$\times 10^6$]	0.22	0.14	0.22	0.22	0.11	0.11	0.04
	K_X/K_{C60p}	7.58	4.57	7.58	7.58	3.86	3.86	1.18
	K_X/K_{Xmin}	6.40	3.86	6.40	6.40	3.26	3.26	1.00
S-Histidyl	ΔG [kcal/mol]	-7.30	-7.20	-7.40	-7.40	-6.90	-6.80	-6.20
	K [$\times 10^6$]	0.22	0.19	0.27	0.27	0.11	0.10	0.04
	K_X/K_{C60p}	7.58	6.40	8.97	8.97	3.86	3.26	1.18
	K_X/K_{Xmin}	6.40	5.41	7.58	7.58	3.26	2.75	1.00
S-Phenylalanyl	ΔG [kcal/mol]	-7.50	-6.90	-7.50	-7.70	-7.20	-6.90	-6.20
	K [$\times 10^6$]	0.31	0.11	0.31	0.44	0.19	0.11	0.04
	K_X/K_{C60p}	10.62	3.86	10.62	14.89	6.40	3.86	1.18
	K_X/K_{Xmin}	8.97	3.26	8.97	12.58	5.41	3.26	1.00
S-Tryptophanyl	ΔG [kcal/mol]	-7.50	-7.10	-7.50	-8.10	-7.00	-6.90	-6.40
	K [$\times 10^6$]	0.31	0.16	0.31	0.87	0.14	0.11	0.05
	K_X/K_{C60p}	10.62	5.41	10.62	29.24	4.57	3.86	1.66
	K_X/K_{Xmin}	3.26	3.26	6.40	17.62	2.75	2.33	1.00
S-Tyrosinyl	ΔG [kcal/mol]	-7.70	-7.00	-7.20	-7.70	-6.90	-6.80	-6.30
	K [$\times 10^6$]	0.44	0.14	0.19	0.44	0.11	0.10	0.04
	K_X/K_{C60p}	14.89	4.57	6.40	14.89	3.86	3.26	1.40
	K_X/K_{Xmin}	10.62	3.26	4.57	10.62	2.75	2.33	1.00

The d2 molecule creates the next important complex with FF, having tryptophanyl substituents in positions R₃-R₅. The visualization of its structure is presented in Figure 5c. The 29-fold increase of the binding affinity relative to the reference system, obtained through a set of impacts including stacking interactions, allows for the creation of a characteristic stacking cluster consisting of the isatin core placed between the tryptophanyl aromatic system and the fullerene surface, as well as hydrogen bonds created by nitro and amino groups of the d2 molecule with fullerene substituents.

The final drug considered, namely, the d3 derivative, creates complexes for which the greatest increase in affinity relative to the reference system was observed. The highest binding capacity towards this drug molecule was shown by FFs containing an argininyl substituent in the R₂-R₄-R₆ and R₂-R₆ positions, for which a 95- and 41-fold increase in affinity was noted, respectively (Table 4), compared to the C60_phen molecule. The structures of such complexes are presented in Figure 6a,b. The graphic representation of both systems clearly shows that both complexes are maintained by strong stacking interactions, which is confirmed by the mutual orientation of interacting systems and quite short distances, placed in the scope from 3.51 to 3.73 Å. The next important factor

increasing the stability of both complexes is a large network of hydrogen bonds, which involves all hydrogen-bond acceptors and donors from the isatine core, as well as the nitro group from the benzohydrazide part of the drug molecule. The next interesting complex of the d3 molecule is created with the FF derivative containing tryptophanyl derivatives in R₃-R₅ positions. The structure of such a system is presented in Figure 5d. The nearly 35-fold increase of binding affinity relative to the reference system is supported by stacking interactions involving all aromatic systems of the drug molecule. In the case of such a complex, the benzyhydrazide part of the drug participates in the creation of a stacking cluster observed in the previously analyzed systems. Such a situation is probably related to the presence of the nitro group in the benzyhydrazide fragment of the molecule, which supports the possibility of a hydrogen-bond creation with a tryptophanyl substituent. The last important complex of the d3 molecule is created with FF-R₃-R₅-S-Tyrosinyl, whose structure is presented in Figure 6c. This system exhibits a nearly 21-fold increase in binding affinity when compared to the interactions of the d3 molecule with the reference nanocarrier. In the structure of the complex considered, stacking interactions are observed between aromatic systems of the drug and the phenyl ring and fullerene surface. The significance of these interactions is confirmed by the quite short distances between interacting subunits placed in the scope from 3.49 to 3.62 Å and the planar orientation of interacting subunits. Additional factors that increase the stability of such systems are the hydrogen bonds involving hydroxyl groups from tyrosinyl substituents and both nitro groups of the drug molecule. Presented data, obtained for all complexes created by considered 5-nitroisatine derivatives with chosen FFs, provide a different image than the data presented in the previous work [46], which analyzed the binding capabilities of such nanocarriers relative to the disubstituted isatine derivatives, which contained at least two chemical groups with aromatic rings bound with a centrally localized isatine core. While the binding abilities of fullerene C₆₀ monoderivatives are similar for both groups of drugs, there are significant discrepancies in the case of polysubstituted carriers. In the case of previous studies, the best binding abilities were unquestionably found in systems containing substituents in the R₃-R₅ position, regardless of the type of chemical groups used in the modification. The value clearly indicating this is the (K_X/K_{C60p}) coefficient, defining the ratio of the equilibrium constant describing the tested complex to the reference system. In the case of complexes formed by the previous group of drugs, with nanoparticles having a modification in the R₃-R₅ position, values indicating an increase in binding capacity ranging from 20-fold to even 80.5-fold were obtained (80.5—Lig1-FF-R₃-R₅-S-Tryptophanyl; 41.0—Lig2-FF-R₃-R₅-S-Tryptophanyl; 34.6—Lig1-FF-R₃-R₅-S-Tyrosinyl; 29.2—Lig2-FF-R₃-R₅-S-Phenylalanyl). In the case of most of the other studied complexes created by nanomolecules, an increase in values greater than tenfold was incidentally recorded. The current research indicates that, in the case of drugs containing a smaller number of aromatic systems, the type of functional groups used is more important and their binding abilities can promote carriers with modifications in the R₂-R₄-R₆ or R₂-R₆ positions. The values of the K_X/K_{C60p} coefficient obtained for such complexes indicate a significant increase of binding affinity relative to the reference system (95.31—d3-FF-R₂-R₄-R₆-S-Argininy; 40.98—d3-FF-R₂-R₆-S-Argininy; 24.7—d1-FF R₂-R₄-R₆-S-Phenylalanyl; 20.86—d1-FF-R₂-R₄-R₆-S-Tryptophanyl).

Table 4. The values of the binding affinity ΔG [kcal/mol] of the d3 molecule toward proposed FFs; K [106] represents values of the binding constant; K_X/K_{C60p} represents normalized factors describing the increase of the binding constant relative to the reference structure (C60_phen; $\Delta G = -6.2$ [kcal/mol]; $K = 0.035 \times 10^6$); and K_X/K_{Xmin} represents normalized factors describing the increase of the binding constant relative to the smallest values obtained for functionalized fullerene with a particular substituent.

Localization of Substituents		FF						
		R ₂ -R ₄ -R ₆	R ₂ -R ₄	R ₂ -R ₆	R ₃ -R ₅	R ₂	R ₃	R ₄
S-Lysinyl	ΔG [kcal/mol]	-7.80	-7.50	-7.90	-7.40	-7.10	-6.90	-6.40
	K [$\times 10^6$]	0.52	0.31	0.62	0.27	0.16	0.11	0.05
	K_X/K_{C60p}	14.89	8.97	17.62	7.58	4.57	3.26	1.40
	K_X/K_{Xmin}	10.62	6.40	12.58	5.41	3.26	2.33	1.00
S-Argininyl	ΔG [kcal/mol]	-8.90	-7.70	-8.40	-8.20	-7.50	-7.30	-6.70
	K [$\times 10^6$]	3.34	0.44	1.44	1.02	0.31	0.22	0.08
	K_X/K_{C60p}	95.31	12.58	40.98	29.24	8.97	6.40	2.33
	K_X/K_{Xmin}	40.98	5.41	17.62	12.58	3.86	2.75	1.00
S-Glutamyl	ΔG	-7.30	-6.90	-7.20	-7.40	-6.90	-6.80	-6.30
	K [$\times 10^6$]	0.22	0.11	0.19	0.27	0.11	0.10	0.04
	K_X/K_{C60p}	6.40	3.26	5.41	7.58	3.26	2.75	1.18
	K_X/K_{Xmin}	5.41	2.75	4.57	6.40	2.75	2.33	1.00
S-Histidyl	ΔG [kcal/mol]	-7.90	-7.30	-7.80	-7.30	-7.30	-7.30	-6.40
	K [$\times 10^6$]	0.62	0.22	0.52	0.22	0.22	0.22	0.05
	K_X/K_{C60p}	17.62	6.40	14.89	6.40	6.40	6.40	1.40
	K_X/K_{Xmin}	12.58	4.57	10.62	4.57	4.57	4.57	1.00
S-Phenylalanyl	ΔG [kcal/mol]	-7.60	-7.20	-7.70	-7.70	-7.20	-7.00	-6.40
	K [$\times 10^6$]	0.37	0.19	0.44	0.44	0.19	0.14	0.05
	K_X/K_{C60p}	10.62	5.41	12.58	12.58	5.41	3.86	1.40
	K_X/K_{Xmin}	7.58	3.86	8.97	8.97	3.86	2.75	1.00
S-Tryptophanyl	ΔG [kcal/mol]	-7.60	-7.50	-7.50	-8.30	-7.10	-7.30	-6.60
	K [$\times 10^6$]	0.37	0.31	0.31	1.21	0.16	0.22	0.07
	K_X/K_{C60p}	10.62	8.97	8.97	34.62	4.57	6.40	1.96
	K_X/K_{Xmin}	5.41	4.57	4.57	17.62	2.33	3.26	1.00
S-Tyrosinyl	ΔG [kcal/mol]	-7.80	-7.70	-7.40	-8.00	-7.10	-7.10	-6.50
	K [$\times 10^6$]	0.52	0.44	0.27	0.73	0.16	0.16	0.06
	K_X/K_{C60p}	14.89	12.58	7.58	20.86	4.57	4.57	1.66
	K_X/K_{Xmin}	8.97	7.58	4.57	12.58	2.75	2.75	1.00

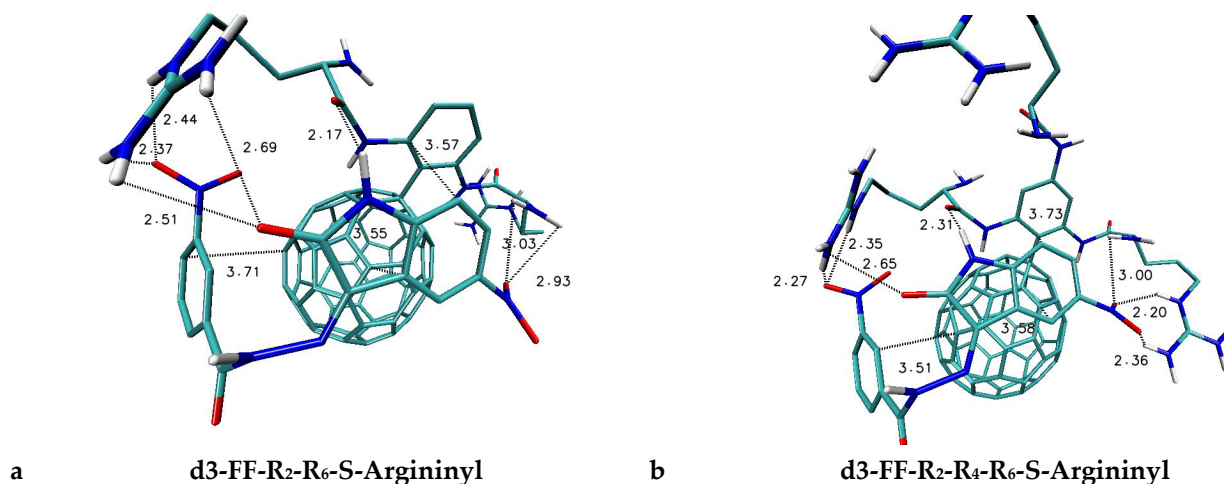


Figure 6. Cont.

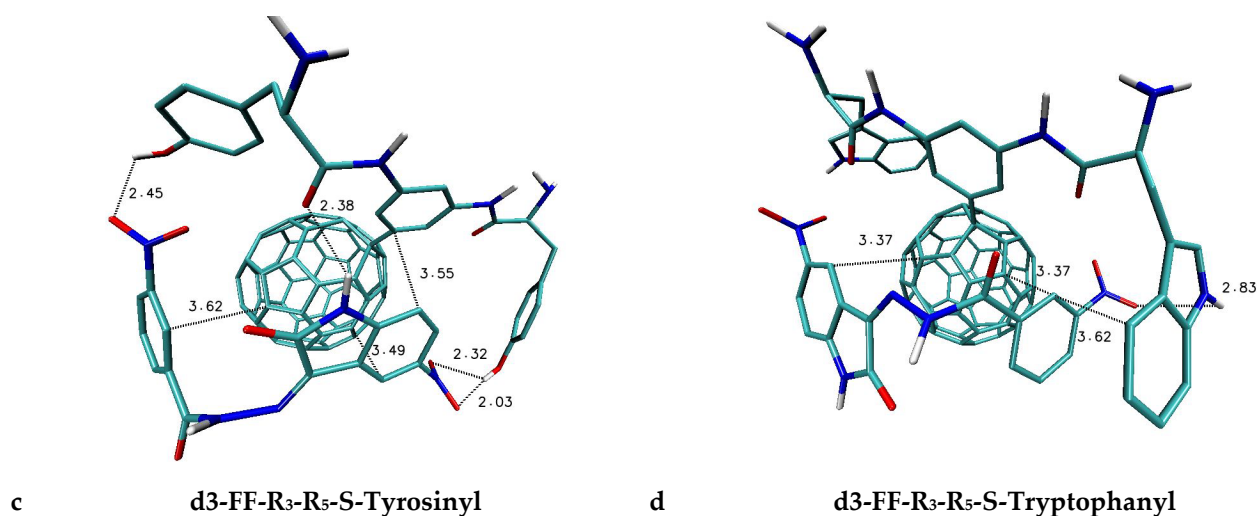


Figure 6. The graphic representation of the chosen complexes created by the d3 molecule with FFs characterized by higher values of binding affinity. The atoms of particular chemical elements are indicated by following colors: carbon—cyan; oxygen—red; nitrogen—blue; and hydrogen—white.

4. Conclusions

Based on the data presented in this paper, it can be unequivocally stated that, within the group of functionalized fullerenes under consideration, nanoparticles with a significant affinity for the studied group of drugs can be distinguished and the formed complexes are stabilized by various types of interactions, including both stacking interactions and hydrogen bonds. In the case of nanocarriers with multiple modifications in the phenyl ring, the factor determining the binding capacity of the considered drugs was the type of chemical substituent used. One type of configuration providing the best binding capacity cannot be unequivocally indicated, as was the case for studies carried out for disubstituted isatin derivatives containing three aromatic systems in their structure. In the case of all drugs considered in this study, the highest binding capacity was found for FFs containing argininy and tryptophanyl modifications. In the case of the first substituent, nanocarrier configurations with substituents located in the R₂-R₄-R₆ and R₂-R₆ positions were promoted, while the most preferred locations of the tryptophanyl groups were the R₃-R₅ positions, which enabled the formation of staking clusters including the aromatic system of the drug, located between the surface of the fullerene and the aromatic system of the substituent. Among the systems with the highest affinity, the dominant systems are complexes created by functionalized fullerenes containing substituents with a symmetrical location, such as R₂-R₆ and R₃-R₅. Based on the collected data, nanocarriers with a high potential for immobilization and use in the development of targeted therapies can be selected for each of the tested drugs. However, further studies that consider more advanced molecular modeling and experiments are necessary to examine the full potential of the tested nanocarriers.

Author Contributions: Conceptualization, P.C., B.S. and A.S.; methodology, P.C.; software, P.C.; validation, P.C.; formal analysis, P.C.; investigation, P.C.; resources, P.C.; data curation, P.C.; writing—original draft preparation, P.C.; writing—review and editing, P.C., B.S. and A.S.; visualization, P.C.; supervision, P.C.; project administration, P.C.; funding acquisition, B.S. All authors have read and agreed to the published version of the manuscript.

Funding: This research received no external funding.

Institutional Review Board Statement: Not applicable.

Informed Consent Statement: Not applicable.

Data Availability Statement: The data are contained within the article.

Acknowledgments: This research was supported by PL-Grid Infrastructure (<http://www.plgrid.pl/en>, accessed on 7 December 2022).

Conflicts of Interest: The authors declare that there are no conflict of interest.

References

1. Zhang, Y.; Du, H.; Liu, H.; He, Q.; Xu, Z. Isatin dimers and their biological activities. *Arch. Pharm.* **2020**, *353*, 1900299. [[CrossRef](#)]
2. Eldehna, W.M.; El Hassab, M.A.; Abo-Ashour, M.F.; Al-Warhi, T.; Elaasser, M.M.; Safwat, N.A.; Suliman, H.; Ahmed, M.F.; Al-Rashood, S.T.; Abdel-Aziz, H.A.; et al. Development of isatin-thiazolo[3,2-a]benzimidazole hybrids as novel CDK2 inhibitors with potent in vitro apoptotic anti-proliferative activity: Synthesis, biological and molecular dynamics investigations. *Bioorg. Chem.* **2021**, *110*, 104748. [[CrossRef](#)]
3. Li, W.; Zhao, S.-J.; Gao, F.; Lv, Z.-S.; Tu, J.-Y.; Xu, Z. Synthesis and In Vitro Anti-Tumor, Anti-Mycobacterial and Anti-HIV Activities of Diethylene-Glycol-Tethered Bis-Isatin Derivatives. *ChemistrySelect* **2018**, *3*, 10250–10254. [[CrossRef](#)]
4. Al-Salem, H.S.; Arifuzzaman, M.; Alkahtani, H.M.; Abdalla, A.N.; Issa, I.S.; Alqathama, A.; Albalawi, F.S.; Rahman, A.F.M.M. A Series of Isatin-Hydrazones with Cytotoxic Activity and CDK2 Kinase Inhibitory Activity: A Potential Type II ATP Competitive Inhibitor. *Molecules* **2020**, *25*, 4400. [[CrossRef](#)] [[PubMed](#)]
5. Ghosh, S.; Ramarao, T.A.; Samanta, P.K.; Jha, A.; Satpati, P.; Sen, A. Triazole based isatin derivatives as potential inhibitor of key cancer promoting kinases- insight from electronic structure, docking and molecular dynamics simulations. *J. Mol. Graph. Model.* **2021**, *107*, 107944. [[CrossRef](#)] [[PubMed](#)]
6. Prakash, C.R.; Theivendren, P.; Raja, S.; Prakash, C.R.; Theivendren, P.; Raja, S. Indolin-2-Ones in Clinical Trials as Potential Kinase Inhibitors: A Review. *Pharmacol. Pharm.* **2012**, *3*, 62–71. [[CrossRef](#)]
7. Ferraz de Paiva, R.E.; Vieira, E.G.; Rodrigues da Silva, D.; Wegermann, C.A.; Costa Ferreira, A.M. Anticancer Compounds Based on Isatin-Derivatives: Strategies to Ameliorate Selectivity and Efficiency. *Front. Mol. Biosci.* **2021**, *7*, 511. [[CrossRef](#)]
8. Katiyar, A.; Hegde, M.; Kumar, S.; Gopalakrishnan, V.; Bhatelia, K.D.; Ananthaswamy, K.; Ramareddy, S.A.; De Clercq, E.; Choudhary, B.; Schols, D.; et al. Synthesis and evaluation of the biological activity of N'-[2-oxo-1,2 dihydro-d3-indol-3-ylidene] benzohydrazides as potential anticancer agents. *RSC Adv.* **2015**, *5*, 45492–45501. [[CrossRef](#)]
9. Guo, H. Isatin derivatives and their anti-bacterial activities. *Eur. J. Med. Chem.* **2019**, *164*, 678–688. [[CrossRef](#)]
10. Elsaman, T.; Mohamed, M.S.; Eltayib, E.M.; Abdel-aziz, H.A.; Abdalla, A.E.; Munir, M.U.; Mohamed, M.A. Isatin derivatives as broad-spectrum antiviral agents: The current landscape. *Med. Chem. Res.* **2022**, *31*, 244–273. [[CrossRef](#)]
11. Xu, Z.; Zhang, S.; Gao, C.; Fan, J.; Zhao, F.; Lv, Z.-S.; Feng, L.-S. Isatin hybrids and their anti-tuberculosis activity. *Chin. Chem. Lett.* **2017**, *28*, 159–167. [[CrossRef](#)]
12. Aboul-Fadl, T.; Abdel-Aziz, H.A.; Abdel-Hamid, M.K.; Elsaman, T.; Thanassi, J.; Pucci, M.J. Schiff Bases of Indoline-2,3-dione: Potential Novel Inhibitors of Mycobacterium Tuberculosis (Mtb) DNA Gyrase. *Molecules* **2011**, *16*, 7864–7879. [[CrossRef](#)] [[PubMed](#)]
13. Thakur, R.K.; Joshi, P.; Baranwal, P.; Sharma, G.; Shukla, S.K.; Tripathi, R.; Tripathi, R.P. Synthesis and antiplasmodial activity of glyco-conjugate hybrids of phenylhydrazono-indolinones and glycosylated 1,2,3-triazolyl-methyl-indoline-2,3-diones. *Eur. J. Med. Chem.* **2018**, *155*, 764–771. [[CrossRef](#)] [[PubMed](#)]
14. Cheke, R.S.; Firke, S.D.; Patil, R.R.; Bari, S.B. ISATIN: New Hope Against Convulsion. *Cent. Nerv. Syst. Agents Med. Chem.* **2018**, *18*, 76–101. [[CrossRef](#)]
15. Emami, S.; Valipour, M.; Kazemi Komishani, F.; Sadati-Ashrafi, F.; Rasoulilian, M.; Ghasemian, M.; Tajbakhsh, M.; Honarchian Masihi, P.; Shakiba, A.; Irannejad, H.; et al. Synthesis, in silico, in vitro and in vivo evaluations of isatin aroylhydrazones as highly potent anticonvulsant agents. *Bioorg. Chem.* **2021**, *112*, 104943. [[CrossRef](#)]
16. Besson, A.; Dowdy, S.F.; Roberts, J.M. CDK Inhibitors: Cell Cycle Regulators and Beyond. *Dev. Cell* **2008**, *14*, 159–169. [[CrossRef](#)] [[PubMed](#)]
17. Czeleń, P. Investigation of the Inhibition Potential of New Oxindole Derivatives and Assessment of Their Usefulness for Targeted Therapy. *Symmetry* **2019**, *11*, 974. [[CrossRef](#)]
18. Czeleń, P. Inhibition mechanism of CDK-2 and GSK-3 β by a sulfamoylphenyl derivative of indoline—A molecular dynamics study. *J. Mol. Model.* **2017**, *23*, 230. [[CrossRef](#)]
19. Czeleń, P. Molecular dynamics study on inhibition mechanism of CDK-2 and GSK-3 β by CHEMBL272026 molecule. *Struct. Chem.* **2016**, *27*, 1807–1818. [[CrossRef](#)]
20. Beauchard, A.; Ferandin, Y.; Frere, S.; Lozach, O.; Blairvacq, M.; Meijer, L.; Thiery, V.; Besson, T. Synthesis of novel 5-substituted indirubins as protein kinases inhibitors. *Bioorg. Med. Chem.* **2006**, *14*, 6434–6443. [[CrossRef](#)]
21. Bramson, H.N.; Holmes, W.D.; Hunter, R.N.; Lackey, K.E.; Lovejoy, B.; Luzzio, M.J.; Montana, V.; Rocque, W.J.; Rusnak, D.; Shewchuk, L.; et al. Oxindole-based inhibitors of cyclin-dependent kinase 2 (CDK2): Design, synthesis, enzymatic activities, and X-ray crystallographic analysis. *J. Med. Chem.* **2001**, *44*, 4339–4358. [[CrossRef](#)] [[PubMed](#)]
22. Czeleń, P.; Skotnicka, A.; Szefer, B. Designing and Synthesis of New Isatin Derivatives as Potential CDK2 Inhibitors. *Int. J. Mol. Sci.* **2022**, *23*, 8046. [[CrossRef](#)] [[PubMed](#)]
23. Gao, Z.; Zhang, L.; Sun, Y. Nanotechnology applied to overcome tumor drug resistance. *J. Control. Release* **2012**, *162*, 45–55. [[CrossRef](#)] [[PubMed](#)]

24. Turov, V.V.; Chehun, V.F.; Barvinchenko, V.N.; Krupskaya, T.V.; Prylutskiy, Y.I.; Scharff, P.; Ritter, U. Low-temperature ¹H-NMR spectroscopic study of doxorubicin influence on the hydrated properties of nanosilica modified by DNA. *J. Mater. Sci. Mater. Med.* **2011**, *22*, 525–532. [[CrossRef](#)] [[PubMed](#)]
25. Morgen, M.; Bloom, C.; Beyerinck, R.; Bello, A.; Song, W.; Wilkinson, K.; Steenwyk, R.; Shamblin, S. Polymeric Nanoparticles for Increased Oral Bioavailability and Rapid Absorption Using Celecoxib as a Model of a Low-Solubility, High-Permeability Drug. *Pharm. Res.* **2012**, *29*, 427–440. [[CrossRef](#)]
26. De Jong, W.H.; Borm, P.J.A. Drug delivery and nanoparticles: applications and hazards. *Int. J. Nanomed.* **2008**, *3*, 133–149. [[CrossRef](#)]
27. Damascelli, B.; Patelli, G.L.; Lanocita, R.; Tolla, G.D.; Frigerio, L.F.; Marchianò, A.; Garbagnati, F.; Spreafico, C.; Tichà, V.; Gladin, C.R.; et al. A Novel Intraarterial Chemotherapy Using Paclitaxel in Albumin Nanoparticles to Treat Advanced Squamous Cell Carcinoma of the Tongue: Preliminary Findings. *Am. J. Roentgenol.* **2003**, *181*, 253–260. [[CrossRef](#)]
28. Alyautdin, R.N.; Petrov, V.E.; Langer, K.; Berthold, A.; Kharkevich, D.A.; Kreuter, J. Delivery of loperamide across the blood-brain barrier with polysorbate 80-coated polybutylcyanoacrylate nanoparticles. *Pharm. Res.* **1997**, *14*, 325–328. [[CrossRef](#)]
29. Kreuter, J.; Ränge, P.; Petrov, V.; Hamm, S.; Gelperina, S.E.; Engelhardt, B.; Alyautdin, R.; von Briesen, H.; Begley, D.J. Direct evidence that polysorbate-80-coated poly(butylcyanoacrylate) nanoparticles deliver drugs to the CNS via specific mechanisms requiring prior binding of drug to the nanoparticles. *Pharm. Res.* **2003**, *20*, 409–416. [[CrossRef](#)]
30. Weissenböck, A.; Wirth, M.; Gabor, F. WGA-grafted PLGA-nanospheres: Preparation and association with Caco-2 single cells. *J. Control. Release* **2004**, *99*, 383–392. [[CrossRef](#)]
31. Dyer, A.M.; Hinchcliffe, M.; Watts, P.; Castile, J.; Jabbal-Gill, I.; Nankervis, R.; Smith, A.; Illum, L. Nasal delivery of insulin using novel chitosan based formulations: A comparative study in two animal models between simple chitosan formulations and chitosan nanoparticles. *Pharm. Res.* **2002**, *19*, 998–1008. [[CrossRef](#)] [[PubMed](#)]
32. Huang, M.; Khor, E.; Lim, L.-Y. Uptake and cytotoxicity of chitosan molecules and nanoparticles: Effects of molecular weight and degree of deacetylation. *Pharm. Res.* **2004**, *21*, 344–353. [[CrossRef](#)] [[PubMed](#)]
33. Gupta, M.; Gupta, A.K. Hydrogel pullulan nanoparticles encapsulating pBUDLacZ plasmid as an efficient gene delivery carrier. *J. Control. Release* **2004**, *99*, 157–166. [[CrossRef](#)] [[PubMed](#)]
34. Szeffler, B. Nanotechnology, from quantum mechanical calculations up to drug delivery. *Int. J. Nanomed.* **2018**, *13*, 6143–6176. [[CrossRef](#)]
35. Cataldo, F.; Da Ros, T. *Medicinal Chemistry and Pharmacological Potential of Fullerenes and Carbon Nanotubes*; Springer: Cham, Switzerland, 2008; ISBN 9781402068454.
36. Panchuk, R.R.; Prylutska, S.V.; Chumakl, V.V.; Skorokhyd, N.R.; Lehka, L.V.; Evstigneev, M.P.; Prylutskiy, Y.I.; Berger, W.; Heffeter, P.; Scharff, P.; et al. Application of C60 Fullerene-Doxorubicin Complex for Tumor Cell Treatment In Vitro and In Vivo. *J. Biomed. Nanotechnol.* **2015**, *11*, 1139–1152. [[CrossRef](#)]
37. Andrievsky, G.; Klochkov, V.; Derevyanchenko, L. Is the C₆₀ Fullerene Molecule Toxic?! *Fuller. Nanotub. Carbon Nanostruct.* **2005**, *13*, 363–376. [[CrossRef](#)]
38. D’Rozario, R.S.G.; Wee, C.L.; Jayne Wallace, E.; Sansom, M.S.P. The interaction of C₆₀ and its derivatives with a lipid bilayer via molecular dynamics simulations. *Nanotechnology* **2009**, *20*, 115102. [[CrossRef](#)]
39. Qiao, R.; Roberts, A.P.; Mount, A.S.; Klaine, S.J.; Ke, P.C. Translocation of C60 and Its Derivatives Across a Lipid Bilayer. *Nano Lett.* **2007**, *7*, 614–619. [[CrossRef](#)]
40. Prylutska, S.; Bilyy, R.; Overchuk, M.; Bychko, A.; Andreichenko, K.; Stoika, R.; Rybalchenko, V.; Prylutskiy, Y.; Tsierkezos, N.G.; Ritter, U. Water-soluble pristine fullerenes C60 increase the specific conductivity and capacity of lipid model membrane and form the channels in cellular plasma membrane. *J. Biomed. Nanotechnol.* **2012**, *8*, 522–527. [[CrossRef](#)]
41. Schuetze, C.; Ritter, U.; Scharff, P.; Fernekorn, U.; Prylutska, S.; Bychko, A.; Rybalchenko, V.; Prylutskiy, Y. Interaction of N-fluorescein-5-isothiocyanate pyrrolidine-C60 with a bimolecular lipid model membrane. *Mater. Sci. Eng. C* **2011**, *31*, 1148–1150. [[CrossRef](#)]
42. Yang, X.; Ebrahimi, A.; Li, J.; Cui, Q. Fullerene-biomolecule conjugates and their biomedical applications. *Int. J. Nanomed.* **2014**, *9*, 77–92. [[CrossRef](#)] [[PubMed](#)]
43. Montellano, A.; Da Ros, T.; Bianco, A.; Prato, M. Fullerene C60 as a multifunctional system for drug and gene delivery. *Nanoscale* **2011**, *3*, 4035. [[CrossRef](#)] [[PubMed](#)]
44. Czeleń, P.; Szeffler, B. The Immobilization of ChEMBL474807 Molecules Using Different Classes of Nanostructures. *Symmetry* **2019**, *11*, 980. [[CrossRef](#)]
45. Kornev, A.B.; Khakina, E.A.; Troyanov, S.I.; Kushch, A.A.; Peregudov, A.; Vasilchenko, A.; Deryabin, D.G.; Martynenko, V.M.; Troshin, P.A. Facile preparation of amine and amino acid adducts of [60]fullerene using chlorofullerene C60Cl6 as a precursor. *Chem. Commun.* **2012**, *48*, 5461. [[CrossRef](#)] [[PubMed](#)]
46. Czeleń, P.; Szeffler, B. The Immobilization of Oxindole Derivatives Using New Designed Functionalized C60 Nanomolecules. *Symmetry* **2020**, *12*, 636. [[CrossRef](#)]
47. Rajendran, V.; Gopalakrishnan, C.; Sethumadhavan, R. Pathological role of a point mutation (T315I) in BCR-ABL1 protein-A computational insight. *J. Cell. Biochem.* **2018**, *119*, 918–925. [[CrossRef](#)]
48. Al-Subaie, A.M.; Kamaraj, B. The Structural Effect of FLT3 Mutations at 835th Position and Their Interaction with Acute Myeloid Leukemia Inhibitors: In Silico Approach. *Int. J. Mol. Sci.* **2021**, *22*, 7602. [[CrossRef](#)]

49. Kamaraj, B.; Al-Subaie, A.M.; Ahmad, F.; Surapaneni, K.M.; Alsamman, K. Effect of novel leukemia mutations (K75E & E222K) on interferon regulatory factor 1 and its interaction with DNA: Insights from molecular dynamics simulations and docking studies. *J. Biomol. Struct. Dyn.* **2021**, *39*, 5235–5247.
50. Rajendran, V.; Sethumadhavan, R. Drug resistance mechanism of PncA in Mycobacterium tuberculosis. *J. Biomol. Struct. Dyn.* **2014**, *32*, 209–221. [[CrossRef](#)]
51. PubChem. Available online: <https://pubchem.ncbi.nlm.nih.gov/> (accessed on 1 May 2019).
52. Lee, C.; Yang, W.; Parr, R.G. Development of the Colle-Salvetti correlation-energy formula into a functional of the electron density. *Phys. Rev. B* **1988**, *37*, 785–789. [[CrossRef](#)]
53. Becke, A.D. Density-functional thermochemistry. III. The role of exact exchange. *J. Chem. Phys.* **1993**, *98*, 5648–5652. [[CrossRef](#)]
54. Ong, B.K.; Woon, K.L.; Ariffin, A. Evaluation of various density functionals for predicting the electrophosphorescent host HOMO, LUMO and triplet energies. *Synth. Met.* **2014**, *195*, 54–60. [[CrossRef](#)]
55. Petersson, G.A.; Bennett, A.; Tensfeldt, T.G.; Al-Laham, M.A.; Shirley, W.A.; Mantzaris, J. A complete basis set model chemistry. I. The total energies of closed-shell atoms and hydrides of the first-row elements. *J. Chem. Phys.* **1988**, *89*, 2193–2218. [[CrossRef](#)]
56. Petersson, G.A.; Al-Laham, M.A. A complete basis set model chemistry. II. Open-shell systems and the total energies of the first-row atoms. *J. Chem. Phys.* **1991**, *94*, 6081–6090. [[CrossRef](#)]
57. Marten, B.; Kim, K.; Cortis, C.; Friesner, R.A.; Murphy, R.B.; Ringnalda, M.N.; Sitkoff, D.; Honig, B. New model for calculation of solvation free energies: Correction of self-consistent reaction field continuum dielectric theory for short-range hydrogen-bonding effects. *J. Phys. Chem.* **1996**, *100*, 11775–11788. [[CrossRef](#)]
58. Barone, V.; Cossi, M.; Tomasi, J. A new definition of cavities for the computation of solvation free energies by the polarizable continuum model. *J. Chem. Phys.* **1997**, *107*, 3210–3221. [[CrossRef](#)]
59. Frisch, M.J.; Trucks, G.W.; Schlegel, H.B.; Scuseria, G.E.; Robb, M.A.; Cheeseman, J.R.; Scalmani, G.; Barone, V.; Petersson, G.A.; Nakatsuji, H.; et al. Gaussian 09, Revision A.02, 2016. Gaussian.com. Available online: <http://gaussian.com/g09citation/> (accessed on 7 December 2017).
60. Lu, T.; Chen, F. Multiwfn: A multifunctional wavefunction analyzer. *J. Comput. Chem.* **2012**, *33*, 580–592. [[CrossRef](#)]
61. Trott, O.; Olson, A.J. AutoDock Vina: Improving the speed and accuracy of docking with a new scoring function, efficient optimization, and multithreading. *J. Comput. Chem.* **2009**, *31*, 455–461. [[CrossRef](#)]
62. Bartashevich, E.V.; Potemkin, V.A.; Grishina, M.A.; Belik, A.V. A Method for Multiconformational Modeling of the Three-Dimensional Shape of a Molecule. *J. Struct. Chem.* **2002**, *43*, 1033–1039. [[CrossRef](#)]
63. Humphrey, W.; Dalke, A.; Schulten, K. VMD: Visual molecular dynamics. *J. Mol. Graph.* **1996**, *14*, 33–38. [[CrossRef](#)]

Disclaimer/Publisher’s Note: The statements, opinions and data contained in all publications are solely those of the individual author(s) and contributor(s) and not of MDPI and/or the editor(s). MDPI and/or the editor(s) disclaim responsibility for any injury to people or property resulting from any ideas, methods, instructions or products referred to in the content.